Rapid Communications | Editors' Suggestion

From latent ferroelectricity to hyperferroelectricity in alkali lead halide perovskites

Guido Roma [*]
Université Paris-Saclay, CEA, Service de Recherches de Métallurgie Physique, 91191 Gif sur Yvette, France

Arthur Marronnier [†]
LPICM, CNRS, École Polytechnique, Université Paris-Saclay, F-91128 Palaiseau, France

Jacky Even
Univ Rennes, INSA Rennes, CNRS, Institut FOTON, UMR 6082, F-35000 Rennes, France

(Received 14 January 2020; accepted 21 August 2020; published 11 September 2020)

Using first principles calculations we show that several alkali lead halides potentially present collective ferroelectric polarization. This should occur at least at the nanoscale; it could be detected macroscopically provided it is not concealed by lattice vibrations in the temperature range of stability of the cubic perovskite phase. For potassium lead halides and for alkali lead fluorides, remarkably, the ferroelectric behavior turns hyperferroelectric, suggesting a more robust ferroelectric polarization in spite of depolarization potentials induced by charge accumulation on surfaces or interfaces.

DOI: 10.1103/PhysRevMaterials.4.092402

Ferroelectricity arises from cooperative polar distortions that stabilize a noncentrosymmetric crystalline structure. An electric field beyond a given threshold can collectively flip the dipole moments associated with the local distortions, which leads to hysteresis in the polarization/electric field curve. When thermal fluctuations are sufficient to destroy long range correlations between the orientation of local dipoles, the crystal becomes paraelectric, keeping however an enhanced dielectric susceptibility in a given range of electric fields. While oxide perovskites have been largely studied for their ferroelectric or paraelectric behavior [1,2], halide perovskites are intensively studied recently for optical devices, spintronics, and photovoltaic applications, in particular hybrid organic-inorganic ones. In the latter, the A cation in the ABX_3 perovskite structure is a small organic molecule whose dipole moment, if aligned in a periodic arrangement, can produce ferroelectricity [3].

Early experiments conducted at room temperature showed that the orientations of the molecular cations correspond to a paraelectric phase for $CH_3NH_3PbI_3$ [4] (methylammonium lead iodide or $MAPbI_3$). Theoretically [5], dipole orientations are shown to be random in the high temperature cubic phase. But the structural phase transition from the high temperature cubic to room temperature tetragonal phase of $CH_3NH_3PbI_3$ is almost impossible to properly simulate by using *ab initio* molecular dynamics, due to the limitations of computational resources. When lowering the temperature, the orthorhombic phase is usually obtained by these methods before the long-range correlations characteristic of the tetragonal phase can be characterized. Recent experiments have shown that $MAPbI_3$ (unlike $MAPbBr_3$) is pyroelectric in its tetragonal phase, at room temperature, and ferroelectricity was further demonstrated at $T = 204$ K by showing an hysteresis loop in the polarization versus electric field curve [6]. Similar results have been obtained for layered perovskites [7]. For cesium-based inorganic perovskites, recent detailed low-temperature single-crystal structural analyses report on both local and long-range centrosymmetric structures [8,9], despite a claim about the observation of hysteresis loops in pressed disks of quantum dot powders [10].

Focusing on the dipole of the organic moiety has somewhat concealed the contribution of the inorganic framework to the polarization. However, $CsPbF_3$ is an example of an alkali halide perovskite with a polar, ferroelectric, ground state [11,12], and also $CsPbI_3$ presents polar instabilities in some of its phases [13–15], including the cubic, high temperature, perovskite phase. This phase, or the tetragonal one, is stabilized at room temperature using strain [16] in the form of quantum dots [17] or thin films [18], producing highly efficient solar cells, but the room temperature ground state is, in reality, a nonperovskite structure [14,15].

Concerning polar distortions, the lack of inversion symmetry in the distorted structure, together with strong spin-orbit coupling, leads to the Rashba effect that could reduce the recombination rate [19]; exciton binding energy could be very low as a consequence of large dielectric screening associated with the ionic contribution to the dielectric constant [20,21]. The role of these two propositions on carrier dynamics has been downplayed because, for the former, first principles calculations show that the influence of the Rashba effect on recombination is weaker than initially expected, both in hybrid [22,23] and inorganic [24] halide perovskites; for the latter hypothesis, the calculated ionic contribution to the dielectric constant [25] is large but not huge. A third scenario, proposed by Miyata [26], involves polar nanodomains surrounding a

[*]guido.roma@cea.fr
[†]Université Paris-Saclay, CEA, Service de Recherches de Métallurgie Physique, 91191 Gif sur Yvette, France.

ferroelectric large polaron, which could provide a much more effective screening and a potential barrier hindering charge recombination. Several works have discussed the possible role of ferroelectric distortions [27,28], highly anharmonic polar modes leading to dipolar random fluctuations larger than stochastic dipolar molecular rotations [29] competing with octahedral rotations [12,30] in halide perovskites, but a detailed knowledge of internal electric fields and polarization in these materials is still missing and it is necessary in order to develop further any model relying on a supposed ferroelectricity.

In this paper we focus on inorganic alkali lead halide perovskites, keeping Pb in the ABX_3 structure because lead's lone pair seems to be instrumental in stabilizing a polar ground state [12]; we show that all the cubic perovskite phases of $APbX_3$ compounds studied here (A = Cs, Rb, K; X = I, Br, Cl, F) present a ferroelectric behavior, to various degrees, reaching in some cases the hyperferroelectric [31] regime; when ferroelectricity, or hyperferroelectricity, is wiped out by thermal fluctuations (which is apparently the case for the α phase of $CsPbI_3$ in its stability domain) the material is paraelectric, or *hyperparaelectric*, but conserves the internal polar distortions typical of normal, or hyper, ferroelectrics, now showing up as dynamical fluctuations of local dipole moments.

Our approach is based on density functional theory (DFT) calculations of four crucial quantities along the distortion pattern of a soft polar phonon: The Kohn-Sham total energy U, the unit cell volume Ω, the polarization P, and the dielectric constant in the high frequency limit ε_∞. The dielectric constant is obtained with density functional perturbation theory [32], and the polarization is obtained with the Berry phase approach [33]. We used the QUANTUM ESPRESSO package [34] for the calculation of the four ingredients of the model within the local density approximation (LDA). We used scalar relativistic norm conserving pseudopotentials with 14 valence electrons for Pb and 9 for all alkali atoms, as for our previous works on $CsPbI_3$ [13,14]. An energy cutoff of 100 Rydberg, **k**-point mesh of size $8 \times 8 \times 8$, and strict threshold for forces (10^{-4} Ryd/Bohr) were used. The Berry phase calculations of the polarization were performed as an integral over a path in reciprocal space containing 20 **k** points in the relevant (k_x) direction, averaged over a 8×8 mesh in the $k_y k_z$ plane. Here, using the LDA, no long range correlation contributions to the energy functional (i.e., no van der Waals terms), were included. Although they may indeed influence the equilibrium lattice constants of hybrid perovskites [35] and maybe also $CsPbI_3$ [36] in combination with gradient corrected functionals, they should not crucially affect the shape of the energy landscape and associated vibrational properties [37] calculated with LDA and thus we neglect them for the fully inorganic perovskites studied in this work. Further checks on the approximations used, including the role of spin orbit coupling [38], are presented in the Supplemental Material [39].

We describe the atomic displacements along the soft phonon previously described for $CsPbI_3$ [13] with a parameter, λ: We define $\lambda = 0$ for the centrosymmetric structure (with space group $Pm\bar{3}m$) and $\lambda = 1$ for the distorted minimum energy configuration. Intermediate configurations are obtained by linear interpolation between symmetric and asymmetric structures. We fit $U(\lambda)$ with a sixth order polynomial with even powers of λ, as in our previous studies of $CsPbI_3$ [13,14]. For the fitting of polarization *vs* λ we use an odd polynomial of fifth degree, for the susceptibility an even combination of Chebyshev polynomials up to the eighth degree.

All twelve $APbX_3$ compounds present the same double well profile of the total energy, $U(\lambda)$, around the symmetric $Pm\bar{3}m$ structure previously described for $CsPbI_3$ [see Fig. 1(a)]. The energy barriers of the double well range from 9 meV for $CsPbBr_3$ to 326 meV for $KPbF_3$ [Fig. 1(b)]. The displacement along one of the three degenerate soft polar phonons (we choose the x direction) leads to a tetragonal distortion and a slight volume expansion for all compounds except the three fluorides, which contract [Fig. 1(c)]; this feature underlines a possible coupling between optical and acoustic phonons.

Coupling between polar and nonpolar distortions may affect the nature of the ferroelectric behavior and the presence of a soft polar phonon does not mean automatically ferroelectricity. A deeper understanding can be gained by studying the electric equation of state, relating the electric field and either the polarization P or the electric displacement D. We consider

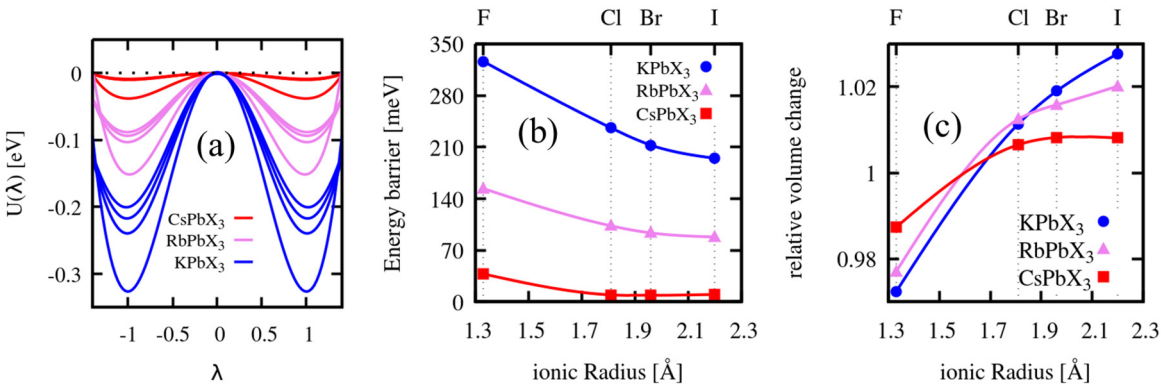

FIG. 1. (a) Total energy profiles $U(\lambda)$, where λ parametrizes the ferroelectric distortion along the soft polar phonon eigenvector. (b) Potential energy barriers U(0)-U(1), of the profiles in (a), plotted vs the ionic radius of the halogen atom [40]. (c) Relative volume change between the asymmetric and symmetric configuration: $\Omega(\lambda = 1)/\Omega(\lambda = 0)$.

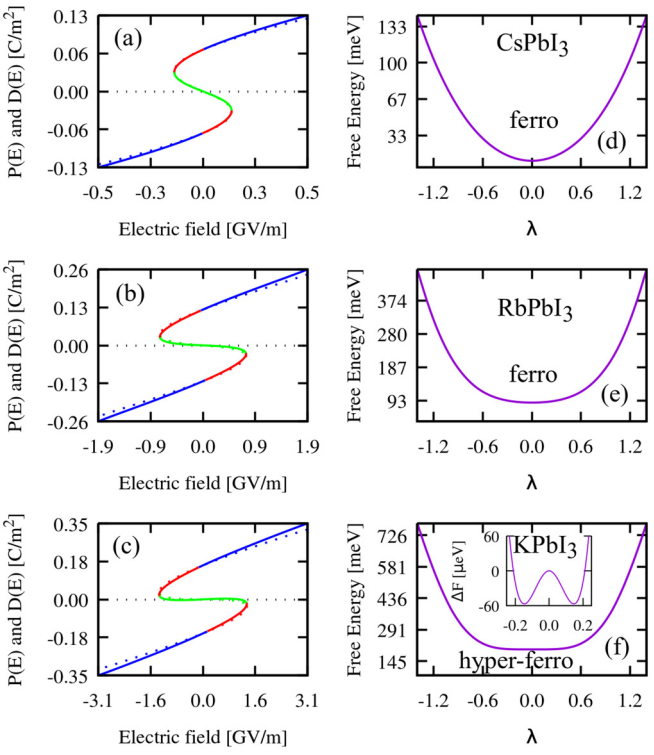

FIG. 2. Panels (a)–(c): The electric displacement field (full line) and the polarization (dotted line) vs electric field curves for the three alkali lead iodides $CsPbI_3$ (a), $RbPbI_3$ (b), and $KPbI_3$ (c). Panels (d)–(f): The electric energy F in open circuit boundary conditions (OCBC) vs the parameter λ for the same compounds. While $CsPbI_3$ and $RbPbI_3$ behave as a normal proper ferroelectric, with a single minimum in the $F(\lambda)$ curve, potassium lead iodide shows incipient hyperferroelectricity [see the zoom in the inset of panel (f)].

the electric energy functional expression [41] for a solid in an external electric field E, as proposed in Ref. [42]:

$$F(\lambda, E) = U(\lambda) - \Omega(\lambda)\left[P(\lambda)E + \frac{1}{8\pi}\chi_\infty(\lambda)E^2\right], \quad (1)$$

where we assumed atomic units, substituting $\varepsilon_0 = \frac{1}{4\pi}$ for the dielectric constant of free space.

In addition to the total energy U and the volume Ω, the expression contains also the polarization P and the electronic susceptibility $\chi_\infty = \varepsilon_\infty - 1$, which were both calculated for various λ, $0 < \lambda < 1.4$, and fitted with polynomials. From these ingredients we can obtain the electric field by solving the second degree equation minimizing the electric energy functional ($\frac{\partial F(\lambda)}{\partial \lambda} = 0$) [42] and, with it, obtain the parametric P-E and D-E curves, i.e., the electric equation of state.

Let us consider first the three iodides: The parametric P-E (or D-E) curves shown in Figs. 2(a)–2(c) present the typical S shape associated with the hysteresis in ferroelectric materials, confirming the potential ferroelectric behavior of these cubic perovskite phases. We use the red/green/blue colors to distinguish the locally stable, locally unstable, and globally stable regions, respectively, which correspond to λ values where $\frac{\partial^2 U}{\partial \lambda^2} > 0$ and $|\lambda| < 1$ (locally stable), $\frac{\partial^2 U}{\partial \lambda^2} < 0$ (locally unstable), and $\frac{\partial^2 U}{\partial \lambda^2} > 0$ and $|\lambda| > 1$ (globally stable). The shape of the curves evolves from $CsPbI_3$ to $KPbI_3$, widening progressively the range of electric fields spanned by the unstable region.

The Kohn-Sham total energy double well profile, as well as the volume, polarization, and dielectric constant, are obtained with calculations at zero field ($E = 0$) and within short circuit boundary conditions (SCBC), which means that the electric field vanishes at the hypothetical surface of an infinite bulk described within periodic boundary conditions. Experimentally, this corresponds to a macroscopic sample where the surfaces are kept at the same potential. Conversely, in several experimental situations implementing open circuit boundary conditions (OCBC), charges accumulate at the surface and induce a depolarization field which counters the buildup of polarization inside the sample. In practice, the polar ground state is at least partially destroyed by the depolarization field. This effect can be predicted by inspecting the electric energy in OCBC [42]:

$$F(\lambda) = U(\lambda) - \Omega(\lambda)\left\{-\frac{4\pi P(\lambda)^2}{1+\chi_\infty(\lambda)} + \frac{1}{2}\chi_\infty(\lambda)\frac{4\pi P(\lambda)^2}{[1+\chi_\infty(\lambda)]^2}\right\} \quad (2)$$

which will show a double well instability only if the depolarization field is not sufficient to destroy the bulk polarization. In panels (d)–(f) of Fig. 2 we show the electric energy in OCBC alongside with the $P(E)$ and $D(E)$ curves previously discussed. The electric energy in OCBC presents a single minimum for $CsPbI_3$ and $RbPbI_3$ but has still a (very shallow) double well profile for $KPbI_3$. This double well is the signature of what has been called a hyperferroelectric [31]: A material which is able to keep a bulk ferroelectric polarization in spite of the depolarization field induced by surface charge accumulation.

In a similar way we can analyze the trend while varying the halogen atom. For the sake of illustration we show in Fig. 3 caesium lead halides, where the evolution from iodide to fluoride is stronger. Starting from $CsPbI_3$, where the ferroelectric behavior stands on a shallow double well for U(λ) whose energy barrier is only on the order of 10 meV [see Figs. 1(a) and 1(b)], we end up with $CsPbF_3$, with a barrier almost four times larger and whose already discussed ferroelectricity [12] we show to be, in reality, hyperferroelectricity. In between them, $CsPbBr_3$ and $CsPbCl_3$ behave very similarly to $CsPbI_3$.

The hyperferroelectric behavior manifests itself not only in the double well shape of the electric energy in OCBC, but also in the shape of the D-E curves (electric displacement vs electric field), qualitatively very similar to the P-E curves. In normal dielectrics the derivative of the electric displacement vs the electric field (i.e., the static dielectric constant, $\varepsilon_{\text{static}}$) is positive, including when the external electric field vanishes ($\frac{dD}{dE}|_{E=0} > 0$); at the ferroelectric transition, however, the dielectric constant diverges and, for a proper ferroelectric, becomes multivalued (hence comes hysteresis); at the crossing of the $D = 0$ axis (in the unstable region) it becomes negative ($\frac{dD}{dE}|_{E=0} < 0$). If we could progressively tune the shape of the D-E curve from a normal ferroelectric towards a hyperferroelectric, $\frac{dD}{dE}|_{E=0}$ would at some point vanish and become positive in the hyperferroelectric state. We normalize

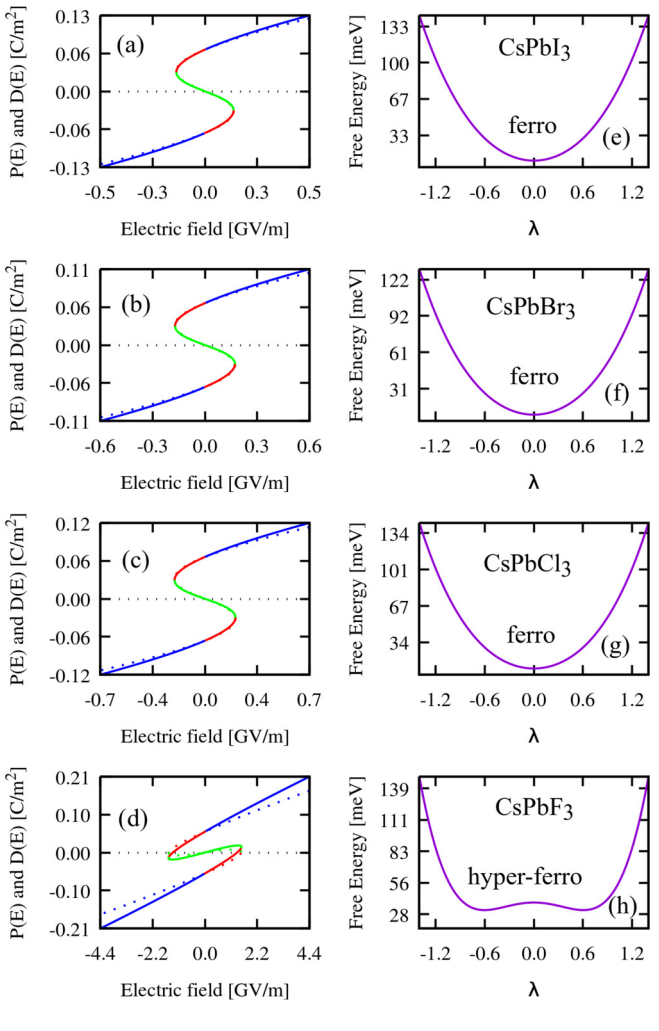

FIG. 3. The electric displacement field (full line) and the polarization (dotted line) vs electric field curves (left column) and the electric energy F in open circuit boundary conditions (OCBC) vs the parameter λ (right column) for the four caesium lead halides: $CsPbI_3$, $CsPbBr_3$, $CsPbCl_3$ and $CsPbF_3$. While the first three behave as normal proper ferroelectrics, with a single minimum in the F(λ) curve, caesium lead fluoride presents a clear hyperferroelectric character.

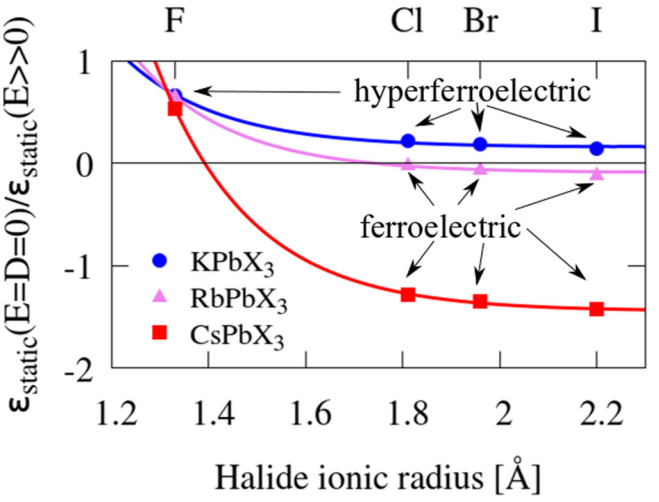

FIG. 4. Normalized static dielectric constant at zero field for alkali lead halides as obtained from our first principles calculations of the *D-E* parametric curves, plotted versus the halogen ionic radius. The lines are a fit of the data with a product of a quadratic function of the alkaline ionic radius and an exponential function of the halogen ionic radius.

this value by the large field linear limit $\frac{dD}{dE}|_{E\gg 0}$, we use it as a measure of the strength of the ferroelectric polarization and follow the trends in the ferroelectricity of alkali lead halides. In Fig. 4 we show the value of $\varepsilon^{E=0}_{\text{static}}/\varepsilon^{E\gg 0}_{\text{static}}$ for the twelve alkali lead halides considered in this paper. For hyperferroelectrics an alternative descriptor is the finite nonzero polarization at zero electric displacement, $P(D=0)$ (see Supplemental Material [39], where P vs D curves, presenting hysteresis only for hyperferroelectrics, are shown).

These results reveal, first, that the trends with alkali substitution, observed in Fig. 2 for the iodides, is maintained for bromides and clorides. Second, all alkali lead fluorides considered here are hyperferroelectric. Third, all potassium lead halides, too, present hyperferroelectric behavior.

$CsPbI_3$ and similar compounds have been shown to be dynamically unstable by harmonic zero temperature phonon calculations [13,43]. The reason is that most of them are found experimentally with the cubic perovskite structure only at relatively high temperatures: $CsPbI_3$ α phase is stable only above 373 °C [14,15], $CsPbCl_3$ assumes the cubic perovskite structure above 47 °C [44] and according to dielectric measurements is not ferroelectric, although Raman measurements show soft phonon modes [45]. $CsPbBr_3$ becomes cubic only above 130 °C [44,46]. The fluoride $CsPbF_3$, conversely, is in the $Pm\bar{3}m$ symmetry at room temperature, transforming to rhombohedral $R3m$ below −83 °C. As far as rubidium compounds are concerned, the bromide has a perovskite structure only above 290 °C [47] and the fluoride above 217 °C [48]. We could not find reports on solid phases of potassium triiodides, except from a citation of $KPbI_3$ as occurring in NH_4CdCl_3-type structure (*Pnma* symmetry) [49].

This tendency to lose the cubic perovskite structure below a certain temperature can be interpreted in terms of the so-called Goldschmidt tolerance factor, useful to assess the tendency of an ABX_3 compound to stabilize in the cubic perovskite structure. Assuming Shannon radii [40] the three alkali lead iodides have tolerance factors ranging from 0.75 (for potassium) to 0.85 (for caesium), somewhere at the lower limit to form perovskite structure. A tolerance factor smaller than one indicates that octahedral tilt rotations can lower the energy of the system, and this explains why several of the compounds considered in this paper have an orthorhombic nonperovskite low temperature ground state and, after intermediate phases, switch to the cubic perovskite structure only at sufficiently high temperature. A mechanism for the transition, as recently shown [50], is due to the temperature evolution of the distribution of tilting angles, which from bimodal at low temperature switches to a single peak at the transition to the cubic phase. It has been suggested that octahedral rotations and ferroelectric distortions are mutually exclusive [30]. The competition between these two mechanisms depends also on how the respective double well depths vary with volume expansion.

TABLE I. Pressure dependence: $\Delta\Omega$ is the difference between the theoretical volume of the asymmetric (symmetric) structure and the experimental value at the lowest temperature of the cubic phase (554 K for $CsPbI_3$ [14] and 148 K for $CsPbF_3$ [11]); ΔU and ΔH are energy and enthalpy differences between symmetric and distorted configuration.

Halide	P (kbar)	$\Delta\Omega$	ΔU	ΔH	$\varepsilon^{E=0}_{\text{static}}$
$CsPbI_3$	0	−5.7% (−4.8%)	10	10	−1.43
	−5	−3.4% (−1.8%)	8	20	−1.05
	−10	−0.3% (+2.1%)	−1	36	−0.88
$CsPbF_3$	0	−2.4% (−3.7%)	38	38	0.54
	−20	+1.6% (+2.2%)	25	33	0.57
	−25	+3.0% (+4.8%)	6	36	0.95

A full understanding of this point would need a thorough study of thermal expansion including anharmonic effects in these materials, however a simpler check is worthwhile: We calculated the depth of the potential well for the ferroelectric distortion at a few negative pressures for $CsPbI_3$ and $CsPbF_3$. The results, summarized in Table I, show that thermal expansion does not affect the crucial features of the energy landscape governing ferroelectricity in these materials.

Independently from the issue of the stability of the cubic phase for each of the considered compounds, we remind that doping hybrid perovskite solar cells with Cs, Rb, and, recently, also K was shown to be beneficial for the stability and performance of halide perovskite solar cells. In particular, potassium doping was shown to improve luminescence [51], reduce hysteresis [52], improve stability, and reduce ion migration [53] by decorating surfaces and grain boundaries. Apart from reducing the band gap and inducing potential beneficial elastic effects—doping with K tends to shrink the lattice parameter—we suggest that potassium could enhance charge separation thanks to a local hyperferroelectric polarization, possibly stabilizing polar nanodomains responsible for the large ferroelectric polaron mechanism [26].

Whether this ferroelectric, or hyperferroelectric, polarization in alkali lead halides is apparent, or latent (paraelectricity or hyperparaelectricity), depends on the role of strongly anharmonic lattice vibrations, which should be investigated in detail for these materials [54]. We might expect a similar ferroelectric behavior in analogous compounds where lead is substituted by other elements in the same column of the periodic table, like Sn, Ge, or Si [30], suggesting further experimental studies on the phase stability of these materials. Finally, we remind that the soft polar phonons which are at the origin of the ferroelectric distortion may also cause a dynamical Rashba effect in $CsPbI_3$ [24], supporting the possibility of an electric field control of the spin texture in alkali lead halide thin films.

In conclusion, using first principles calculations we have shown that several alkali lead halides potentially present collective ferroelectric polarization. This should occur at least at the nanoscale; it could be detected macroscopically provided it is not concealed by lattice vibrations in the temperature range of stability of the cubic perovskite phase. For potassium lead halides and for alkali lead fluorides, remarkably, the ferroelectric behavior turns hyperferroelectric, suggesting a more robust ferroelectric polarization in spite of depolarization potentials induced by charge accumulation on surfaces or interfaces.

This work was granted access to the HPC resources of TGCC under the allocation 2018A0010906018 made by GENCI and under the allocation by CEA-DEN. J.E. acknowledges the financial support from the Institut Universitaire de France.

[1] M. Dawber, K. M. Rabe, and J. F. Scott, Rev. Mod. Phys. **77**, 1083 (2005).
[2] P. Ghosez and J.-M. Triscone, Nat. Mater. **10**, 269 (2011).
[3] J. M. Frost, K. T. Butler, F. Brivio, C. H. Hendon, M. van Schilfgaarde, and A. Walsh, Nano Lett. **14**, 2584 (2014).
[4] Z. Fan, J. Xiao, K. Sun, L. Chen, Y. Hu, J. Ouyang, K. P. Ong, K. Zeng, and J. Wang, J. Phys. Chem. Lett. **6**, 1155 (2015).
[5] J. Even, M. Carignano, and C. Katan, Nanoscale **8**, 6222 (2016).
[6] Y. Rakita, O. Bar-Elli, E. Meirzadeh, H. Kaslasi, Y. Peleg, G. Hodes, I. Lubomirsky, D. Oron, D. Ehre, and D. Cahen, Proc. Natl. Acad. Sci. USA **114**, E5504 (2017).
[7] Q. Zhang, A. Solanki, K. Parida, D. Giovanni, M. Li, T. L. C. Jansen, M. S. Pshenichnikov, and T. C. Sum, ACS Applied Materials & Interfaces **11**, 13523 (2019).
[8] D. B. Straus, S. Guo, A. M. Abeykoon, and R. J. Cava, Adv. Mater. **32**, 2001069 (2020).
[9] M. C. Brennan, M. Kuno, and S. Rouvimov, Inorg. Chem. **58**, 1555 (2019).
[10] X. Li, S. Chen, P.-F. Liu, Y. Zhang, Y. Chen, H.-L. Wang, H. Yuan, and S. Feng, J. Am. Chem. Soc. **142**, 3316 (2020).
[11] P. Berastegui, S. Hull, and S.-G. Eriksson, J. Phys.: Condens. Matter **13**, 5077 (2001).
[12] E. H. Smith, N. A. Benedek, and C. J. Fennie, Inorg. Chem. **54**, 8536 (2015).
[13] A. Marronnier, H. Lee, B. Geffroy, J. Even, Y. Bonnassieux, and G. Roma, J. Phys. Chem. Lett. **8**, 2659 (2017).
[14] A. Marronnier, G. Roma, S. Boyer-Richard, L. Pedesseau, J.-M. Jancu, Y. Bonnassieux, C. Katan, C. C. Stoumpos, M. G. Kanatzidis, and J. Even, ACS Nano **12**, 3477 (2018).
[15] R. J. Sutton, M. R. Filip, A. A. Haghighirad, N. Sakai, B. Wenger, F. Giustino, and H. J. Snaith, ACS Energy Lett. **3**, 1787 (2018).
[16] J. A. Steele, H. Jin, I. Dovgaliuk, R. F. Berger, T. Braeckevelt, H. Yuan, C. Martin, E. Solano, K. Lejaeghere, S. M. J. Rogge, C. Notebaert, W. Vandezande, K. P. F. Janssen, B. Goderis, E. Debroye, Y.-K. Wang, Y. Dong, D. Ma, M. Saidaminov, H. Tan *et al.*, Science **365**, 679 (2019).

[17] A. Swarnkar, A. R. Marshall, E. M. Sanehira, B. D. Chernomordik, D. T. Moore, J. A. Christians, T. Chakrabarti, and J. M. Luther, Science **354**, 92 (2016).

[18] Y. Wang, M. I. Dar, L. K. Ono, T. Zhang, M. Kan, Y. Li, L. Zhang, X. Wang, Y. Yang, X. Gao, Y. Qi, M. Grätzel, and Y. Zhao, Science **365**, 591 (2019).

[19] F. Zheng, L. Z. Tan, S. Liu, and A. M. Rappe, Nano Lett. **15**, 7794 (2015).

[20] J. Even, L. Pedesseau, and C. Katan, J. Phys. Chem. C **118**, 11566 (2014).

[21] A. Miyata, A. Mitioglu, P. Plochocka, O. Portugal, J. T.-W. Wang, S. D. Stranks, and H. J. Snaith, and R. J. Nicholas, Nat. Phys. **11**, 582 (2015).

[22] X. Zhang, J.-X. Shen, and C. G. Van de Walle, J. Phys. Chem. Lett. **9**, 2903 (2018).

[23] X. Zhang, J.-X. Shen, W. Wang, and C. G. Van de Walle, ACS Energy Lett. **3**, 2329 (2018).

[24] A. Marronnier, G. Roma, M. A. Carignano, Y. Bonnassieux, C. Katan, J. Even, E. Mosconi, and F. De Angelis, J. Phys. Chem. C **123**, 291 (2019).

[25] A. Marronnier, H. Lee, H. Lee, M. Kim, C. Eypert, J.-P. Gaston, G. Roma, D. Tondelier, B. Geffroy, and Y. Bonnassieux, Sol. Energy Mater. Sol. Cells **178**, 179 (2018).

[26] K. Miyata and X.-Y. Zhu, Nat. Mater. **17**, 379 (2018).

[27] J. M. Frost, K. T. Butler, and A. Walsh, APL Materials **2**, 081506 (2014).

[28] B. Chen, J. Shi, X. Zheng, Y. Zhou, K. Zhu, and S. Priya, J. Mater. Chem. A **3**, 7699 (2015).

[29] C. Katan, A. D. Mohite, and J. Even, Nat. Mater. **17**, 377 (2018).

[30] S. K. Radha, C. Bhandari, and W. R. L. Lambrecht, Phys. Rev. Materials **2**, 063605 (2018).

[31] K. F. Garrity, K. M. Rabe, and D. Vanderbilt, Phys. Rev. Lett. **112**, 127601 (2014).

[32] S. Baroni, S. de Gironcoli, A. Dal Corso, and P. Giannozzi, Rev. Mod. Phys. **73**, 515 (2001).

[33] R. Resta, Rev. Mod. Phys. **66**, 899 (1994).

[34] P. Giannozzi, S. Baroni, N. Bonini, M. Calandra, R. Car, C. Cavazzoni, D. Ceresoli, G. L. Chiarotti, M. Cococcioni, I. Dabo, A. Dal Corso, S. de Gironcoli, S. Fabris, G. Fratesi, R. Gebauer, U. Gerstmann, C. Gougoussis, A. Kokalj, M. Lazzeri, L. Martin-Samos *et al.*, J. Phys.: Condens. Matter **21**, 395502 (2009).

[35] D. A. Egger and L. Kronik, J. Phys. Chem. Lett. **5**, 2728 (2014).

[36] J. Li and P. Rinke, Phys. Rev. B **94**, 045201 (2016).

[37] M. A. Pérez-Osorio, A. Champagne, M. Zacharias, G.-M. Rignanese, and F. Giustino, J. Phys. Chem. C **121**, 18459 (2017).

[38] J. Even, L. Pedesseau, J.-M. Jancu, and C. Katan, J. Phys. Chem. Lett. **4**, 2999 (2013).

[39] See Supplemental Material at http://link.aps.org/supplemental/10.1103/PhysRevMaterials.4.092402 for some additional VASP [55, 56] calculations with other functionals [57–60] and spin-orbit coupling.

[40] We use Shannon ionic radii, assuming oxidation state +1,+2 and −1 for alkali, lead, and halogens, respectively. The coordination number is 6 for lead and the halogens and 12 for alkali atoms.

[41] M. Stengel, N. A. Spaldin, and D. Vanderbilt, Nat. Phys. **5**, 304 (2009).

[42] R. Adhikari and H. Fu, Phys. Rev. B **99**, 104101 (2019).

[43] R. X. Yang, J. M. Skelton, E. L. da Silva, J. M. Frost, and A. Walsh, J. Chem. Phys. **152**, 024703 (2020).

[44] C. Kn. Møller, Mat. Fys. Medd. Dan. Vid. Selsk. **32**, 2 (1959).

[45] S. Hirotsu, J. Phys. Soc. Jpn. **31**, 552 (1970).

[46] S. Hirotsu, J. Harada, M. Iizumi, and K. Gesi, J. Phys. Soc. Jpn. **37**, 1393 (1974).

[47] B. Tang, Y. Hu, H. Dong, L. Sun, B. Zhao, X. Jiang, and L. Zhang, Angew. Chem., Int. Ed. **58**, 16134 (2019).

[48] Y. Yamane, K. Yamada, and K. Inoue, Sol. State Ionics **179**, 605 (2008).

[49] H. W. Zandbergen, G. C. Verschoor, and D. J. W. Ijdo, Acta Cryst. **B35**, 1425 (1979).

[50] J. S. Bechtel, J. C. Thomas, and A. Van der Ven, Phys. Rev. Materials **3**, 113605 (2019).

[51] M. Abdi-Jalebi, Z. Andaji-Garmaroudi, S. Cacovich, C. Stavrakas, B. Philippe, J. M. Richter, M. Alsari, E. P. Booker, E. M. Hutter, A. J. Pearson, S. Lilliu, T. J. Savenije, H. Rensmo, G. Divitini, C. Ducati, R. H. Friend, and S. D. Stranks, Nature (London) **555**, 497 (2018).

[52] Z. Tang, T. Bessho, F. Awai, T. Kinoshita, M. M. Maitani, R. Jono, T. N. Murakami, H. Wang, T. Kubo, S. Uchida, and H. Segawa, Sci. Rep. **7**, 12183 (2017).

[53] J. K. Nam, S. U. Chai, W. Cha, Y. J. Choi, W. Kim, M. S. Jung, J. Kwon, D. Kim, and J. H. Park, Nano Lett. **17**, 2028 (2017).

[54] O. Yaffe, Y. Guo, L. Z. Tan, D. A. Egger, T. Hull, C. C. Stoumpos, F. Zheng, T. F. Heinz, L. Kronik, M. G. Kanatzidis, J. S. Owen, A. M. Rappe, M. A. Pimenta, and L. E. Brus, Phys. Rev. Lett. **118**, 136001 (2017).

[55] G. Kresse and J. Furthmüller, Phys. Rev. B **54**, 11169 (1996).

[56] G. Kresse and J. Hafner, Phys. Rev. B **47**, 558 (1993).

[57] J. P. Perdew, K. Burke, and M. Ernzerhof, Phys. Rev. Lett. **77**, 3865 (1996).

[58] J. P. Perdew, A. Ruzsinszky, G. I. Csonka, O. A. Vydrov, G. E. Scuseria, L. A. Constantin, X. Zhou, and K. Burke, Phys. Rev. Lett. **100**, 136406 (2008).

[59] J. Heyd, G. E. Scuseria, and M. Ernzerhof, J. Chem. Phys. **118**, 8207 (2003).

[60] J. Heyd, G. E. Scuseria, and M. Ernzerhof, J. Chem. Phys. **124**, 219906 (2006).